Sensing-Driven Spatial Reuse in Shared Spectrum: ns-3 Implementation and Evaluation of Radiation Null Steering

George Frangulea
University of Kent
Canterbury, United Kingdom
gvf3@kent.ac.uk

Philippos Assimakopoulos
University of Kent
Canterbury, United Kingdom
p.asimakopoulos@kent.ac.uk

Sandra Lagén
Centre Tecnològic de Telecomunicacions de Catalunya
Castelldefels, Spain
sandra.lagen@cttc.es

Biljana Bojović
Centre Tecnològic de Telecomunicacions de Catalunya
Castelldefels, Spain
biljana.bojovic@cttc.es

Abstract

Efficient coexistence management is essential for maximising spectrum utilisation in shared 5G New Radio–Unlicensed (NR-U) environments, where heterogeneous radio access technologies compete for the same channel resources. Conventional omnidirectional Listen-Before-Talk (LBT) mitigates persistent interference, yet fails to fully exploit the spatial reuse potential of active antenna arrays in dense deployments. This work introduces a practical null space projected LBT and digital precoder that jointly suppress interference from and toward coexisting nodes while remaining 3GPP- and regulatory-compliant. Implemented in ns-3 and 5G-LENA, system-level simulations demonstrate that the proposed approach enables concurrent transmissions, substantially enhances spatial reuse, and reduces latency compared to legacy LBT schemes.

CCS Concepts

• **Networks** → **Network simulations**; **Mobile networks**.

Keywords

ns-3, NR-U, LBT, Shared Spectrum, Coexistence, Null Steering

ACM Reference Format:
George Frangulea, Philippos Assimakopoulos, Sandra Lagén, and Biljana Bojović. 2025. Sensing-Driven Spatial Reuse in Shared Spectrum: ns-3 Implementation and Evaluation of Radiation Null Steering. In *2025 International Conference on ns-3 (ICNS3 2025), August 19–21, 2025, Osaka, Japan.* ACM, New York, NY, USA, 9 pages. https://doi.org/10.1145/3747204.3747207

1 Introduction

Growing wireless data traffic and diverse use cases drive the need for advanced spectrum sharing [4, 11]. The 3rd Generation Partnership Project (3GPP) addresses this by enabling 5G New Radio-Unlicensed (NR-U) [1] in the sub-7 GHz UNII and 60 GHz mmWave bands, supporting dense deployments but posing significant challenges with other unlicensed systems.

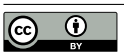

ICNS3 2025, Osaka, Japan

ACM ISBN 979-8-4007-1517-4/25/08
https://doi.org/10.1145/3747204.3747207

Coexistence in NR-U builds on mechanisms such as Listen-Before-Talk (LBT) based Channel Access Procedures (CAPs) for shared spectrum [2]. While these approaches limit persistent interference, they remain contention-based and do not fully exploit the spatial reuse potential available in dense or heterogeneous environments. With spectrum sharing set to play a key role in the upcoming 6G, there is growing consensus that advanced spatial processing, particularly digital precoding and interference suppression techniques, will be critical to maximising efficiency in future wireless networks [12]. This paper investigates practical radiation-null steering for NR-U. While prior theoretical work [8] has shown the potential of interference nulling, such methods typically require base stations to remain silent during interference channel subspace estimation, reducing channel access for cellular users.

In contrast, we propose a novel LBT-based CAP that leverages LBT-sensed snapshots to estimate the interference covariance, which is then used to compute a null space projection matrix. Applying this matrix enables a Secondary Network (SN) gNB to null interference from Primary Network (PN) nodes during LBT, as well as towards PN nodes during Downlink (DL) transmissions via a projected digital precoder. We implement this approach in the open-source ns-3 5G-LENA module and evaluate its effectiveness in a realistic indoor deployment. Our results demonstrate that secondary NR-U base stations can use spatial nulls to protect primary networks while sustaining high DL throughput to their own users, with primary throughput approaching interference-free levels. The source code used in this work is publicly available[1].

The rest of this paper is organised as follows: Section 2 details the system model and precoder design; Section 3 describes the ns-3 implementation; Section 4 presents performance results, and Section 5 concludes the paper.

2 System Setup

We consider two coexisting NR-U networks in an indoor mixed office environment: the PN, where each node uses a single-port omnidirectional antenna, and the SN, where each gNB employs a Uniform Planar Array (UPA) with M horizontal and N vertical antenna elements, yielding $L = M \times N$ spatial degrees of freedom (DoF). Each SN UE may be equipped with a single-port or multi-port omnidirectional antenna. Hence, the i-th SN gNB may transmit up

[1] https://gitlab.com/GeorgeFrangulea/null-space-projection-nru

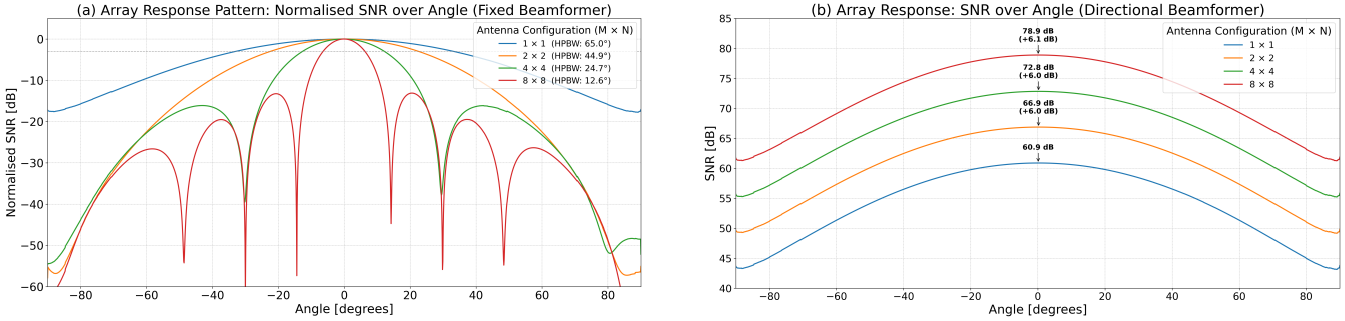

Figure 1: Array Response for Uniform Planar Arrays of Varying Size: (a) Normalised SNR Patterns and Half-Power Beamwidth (HPBW); (b) SNR Gain Improvement

to K_i streams per user on each resource block, with K_i capped by the smallest of the gNB's transmit-port count, the UE's receive-port count, and the instantaneous channel rank under Time Division Duplexing (TDD) reciprocity. In the evaluated system presented in Section 4, we set $K_i = 1$.

The number of antenna ports at the SN gNB sets the array gain and its ability to form narrow beams and deep spatial nulls. As Figure 1 illustrates, a larger array boosts the main-lobe SNR while tightening the half-power beamwidth (HPBW). Results stem from ns-3 simulations with the 3GPP InH-MixedOffice channel model, assuming a transmit power of 24 dBm at the SN gNB and 18 dBm at the UE, with the UE using an isotropic antenna. Measurements were taken in 0.1° steps along a semi-circular UE path, emulating anechoic chamber tests. In Figure 1a, the beamformer is fixed at 0° to show array directivity, sidelobes, and nulls. In Figure 1b the beamformer is recalculated ("steered") at each UE position, so the plot shows the peak SNR achievable in every direction. Notice the sharp SNR drop at ± 90°, where the signal arrives *along* the plane of the panel (grazing incidence), highlighting a planar array's much lower sensitivity to these side directions.

To mitigate interference towards and from (towards/from) neighbouring networks, each i-th SN gNB estimates interference channel conditions through directional sensing performed during the LBT procedure. Subsequently, this information is utilised to construct a precoder projected onto an interference-free subspace. This information is further leveraged in a second stage of the LBT, where directional projected sensing is performed to access the channel based on the energy detected after spatial null placement.

2.1 Digital Precoder with Null Steering

The following steps outline the process for computing a projected precoder that nulls the strongest interfering directions:

Step 1: Interference Covariance Matrix Estimation. During the LBT sensing period, each SN gNB receives signals from active interfering devices (both primary and/or secondary). At the i-th SN gNB the interference-plus-noise covariance matrix $\mathbf{R}_{\text{intf},i}$ is computed from M snapshots collected during the LBT sensing interval:

$$\mathbf{R}_{\text{intf},i} = \frac{1}{M}\sum_{m=1}^{M} \mathbf{z}_i[m]\mathbf{z}_i[m]^H, \tag{1}$$

where $\mathbf{z}_i[m]$ is the snapshot received at symbol index m.

Step 2: Eigenvalue Decomposition. To identify dominant interference directions, decompose $\mathbf{R}_{\text{intf},i}$:

$$\mathbf{R}_{\text{intf},i} = \mathbf{U}_i \mathbf{\Lambda}_i \mathbf{U}_i^H, \tag{2}$$

where $\mathbf{U}_i$ is the eigenvector matrix and $\mathbf{\Lambda}_i$ contains the ordered eigenvalues. The first D_i columns of $\mathbf{U}_i$ form $\mathbf{U}_{\text{intf},i}$, i.e. the strongest interference sub-space at the i-th SN gNB. For convenience, write

$$\mathbf{U}_{\text{intf},i} = \left[\, \mathbf{u}_{\text{intf},i}^{(1)}\ \mathbf{u}_{\text{intf},i}^{(2)}\ \cdots\ \mathbf{u}_{\text{intf},i}^{(D_i)} \right],$$

where $\mathbf{u}_{\text{intf},i}^{(k)} \in \mathbb{C}^{L\times 1}$ *is the* k*-th column* ($k = 1, \ldots, D_i$).

Step 3: Interfering Null Space Projection Matrix.

$$\mathbf{P}_i^{\perp} = \mathbf{I} - \mathbf{U}_{\text{intf},i}\mathbf{U}_{\text{intf},i}^H, \tag{3}$$

where $\mathbf{I}$ is the $L\times L$ identity matrix. *Because the columns* $\mathbf{u}_{\text{intf},i}^{(k)}$ *of* $\mathbf{U}_{\text{intf},i}$ *are obtained from the* Uplink *(UL) (receive-side) sensed samples,* $\mathbf{P}_i^{\perp}$ *satisfies* $\mathbf{P}_i^{\perp}\,\mathbf{u}_{\text{intf},i}^{(k)} = \mathbf{0}$ *for every* k. The choice of D_i must also satisfy $D_i + K_i \le L$ such that K_i data streams remain available for the intended SN UE.

Step 4: Maximum-Ratio Transmission (MRT) Precoder. Let the $\mathbf{H}_{i,\text{gNB}\to\text{UE}}$ denote the DL channel from the i-th SN gNB to its UE. Then, the MRT precoder for gNB i is

$$\mathbf{W}_{\text{MRT},i} = \frac{1}{\gamma_i}\mathbf{H}_{i,\text{gNB}\to\text{UE}}^H, \tag{4}$$

where the scaling factor $\gamma_i = \sqrt{\text{Tr}\left(\mathbf{H}_{i,\text{gNB}\to\text{UE}}^H \mathbf{H}_{i,\text{gNB}\to\text{UE}}\right)}$ normalises the average transmit power to 1.

Step 5: Projected Precoder Calculation. Because $\mathbf{P}_i^{\perp}$ is tailored to null the *UL* steering vectors, we apply its *transpose* so that it suppresses any components of the MRT weights that lie in the DL interference direction(s):

$$\mathbf{W}_{\text{proj},i} = \left(\mathbf{P}_i^{\perp}\right)^T \mathbf{W}_{\text{MRT},i}. \tag{5}$$

(Equivalently, one can choose to project the UL channel $\mathbf{H}_{\text{proj},i} = \mathbf{P}_i^{\perp}\mathbf{H}_{i,\text{UE}\to\text{gNB}}$, transpose to obtain the DL view, and set $\mathbf{W}_{\text{proj},i} = (\mathbf{H}_{\text{proj},i}^T)^H/\gamma_i$.)

2.2 Channel Access Procedure with Null Steering

In compliance with regulatory standards, each gNB must execute Type 1 CAP [7] to access a shared band. The SN gNB operates in two stages:

(1) *Initial directional sensing*. The SN gNB first performs directional sensing for a minimum of 0.3 ms, a duration which can be adjusted to improve the likelihood of capturing all active interferers. During this initial phase, the energy detection (ED) criterion is applied:

$$\|\mathbf{z}_i[m]\|^2 < X_{\text{thresh}}, \qquad m = 1, \ldots, M_{\text{LBT}}. \tag{6}$$

where M_{LBT} is determined by the defer duration plus a random number of backoff sensing slots [7].

(2) *Projected directional sensing*. Using the null space projection matrix from Eq. 3, we test

$$\left\|\mathbf{P}_i^{\perp}\,\mathbf{z}_i[m]\right\|^2 < X_{\text{thresh}}, \qquad m = 1, \ldots, M_{\text{LBT}}. \tag{7}$$

The two-stage LBT procedure first identifies and then suppresses the dominant interference directions during LBT. The same null space projection matrix is used in Eq. 5 to ensure that the same directions are cancelled for the SN gNB DL transmission.

3 Directional Sensing and Precoding with Radiation-Null Steering in ns-3

To evaluate our BF technique with projection onto nulls in a shared spectrum setting, we build upon the ns-3 5G-LENA framework. This discrete-event simulator offers a fully 3GPP-compliant NR protocol stack spanning the PHY, MAC, and upper layers [10], making it ideal for cross-layer coexistence studies. The module has been extensively validated for indoor and outdoor deployments, aligning with 3GPP models [9], and includes critical NR-U features, such as multiple Channel Access Managers, Channel Occupancy Time (COT) sharing, and an unlicensed-mode PHY state machine. Our work builds on recent enhancements to the NR-U module [7] and [6], which include updates to the Type 1 CAP in line with the latest 3GPP TS 37.213 [2] specification.

This section dives into the extensions made to the 5G-LENA simulator framework by going through each modified and added class. Our proposed BF with radiation-null steering extends the closed-loop single-user (SU) MIMO model by integrating the directional LBT sensing procedure to estimate the interference-plus-noise covariance matrix at the gNB and dynamically adjust the precoding matrix for efficient null steering. Figure 2 shows the diagram of the classes that are involved in the computation of the DL precoding matrix, projection matrix and the projected precoding matrix at the gNB. The illustrated classes in Figure 2 are highlighted in blue for newly added classes, in green for significantly modified classes and in grey for classes with little to no change.

3.1 Multiple Transmission Modes Support

We extend the `NrHelper` class to allow multiple networks with gNBs configured for different transmission modes (e.g., *QuasiOmni*[2], *Precoding*[3], and *Codebook*[4]). Before any configuration, a map of gNB nodes, their UEs, and transmission modes is set via the function `NrHelper::SetGnbConfigTypeMap`. This map is referenced in methods such as `CreateUePhy`, `CreateGnbPhy`, and `AttachToEnb` to determine antenna setups, beamforming managers, and other parameters for each gNB–UE pair.

During PHY-layer creation, if the gNB uses *QuasiOmni*, the method `NrHelper::CreateUePhy` registers a callback to function `GenerateDlCqiReport`. Conversely, if the gNB is set for *Precoding*, `GenerateDlCqiReportMimo` is registered instead. During the gNB PHY layer creation in `CreateGnbPhy`, any gNB configured for *Precoding* triggers `NrGnbPhy::GenerateTddMimoPrecoder` and calls `NrSpectrumPhy::AddLbtInterfMimoChunkProcessor` to integrate `NrMimoChunkProcessor` for LBT interference measurement on the sensed multi-antenna signals.

Devices configured for *QuasiOmni* transmission are set with `IsotropicAntennaModel`, while *Precoding* based transmission employs a `ThreeGppAntennaModel`. The parameters, such as the number of antenna ports and polarisation, are set by methods including `SetupOmniUeAntennas` and `SetupDirGnbAntennas`. Finally, in `NrHelper::AttachToEnb`, the selected transmission mode for each gNB-UE pair determines which beamforming algorithm is used. For instance, `CellScanBeamforming` is applied for directional mode, while `QuasiOmniDirectPathBeamforming` is chosen for omnidirectional mode. The appropriate algorithm is set using two helpers: `SetDirBeamformingHelper` or `SetOmniBeamformingHelper`. For *Precoding*, both the gNB and UE maintain a shared `NrPrecoding` object. This object is first configured by calling functions such as `NrPrecodingMethod::SetGnbParams` and `SetUeParams`. The maximum spatial multiplexing rank at the SN gNB is then defined by `NrPrecodingMethod::InitNrPrecoding`.

3.2 Extending PHY and Spectrum Layers

`NrGnbPhy` and `NrUePhy` are the main classes representing the gNB and UE physical layers, respectively. `NrGnbPhy` handles spectrum transmission, scheduling interactions, numerology configuration, and unlicensed channel access while delegating low-level spectrum operations to its associated `NrSpectrumPhy` instance. It manages state transitions and slot timings, communicating with the MAC layer over a SAP interface, and uses a `L1L2CtrlLatency` to model processing delays. Meanwhile, `NrUePhy` executes scheduling and beamforming decisions from the base station, maintaining a state-machine-driven slot-processing model while delegating signal reception, interference handling, and HARQ processes to its own `NrSpectrumPhy` instance.

Since 5G-LENA does not natively support DL precoder computation on the gNB side, as shown in Figure 2, new methods were added to `NrGnbPhy` and `NrUePhy`. Function `GenerateTddMimoPrecoder` processes MIMO signals captured during LBT sensing and provides necessary signals to compute the corresponding precoding matrices. These matrices are shared with UEs via the function `NrUePhy::SetPrecodingMatrix` for CQI report generation. When

[2] Quasi-Omnidirectional transmission

[3] Beamforming using perfect channel knowledge, a.k.a. non-codebook-based precoding

[4] Beamforming from a predefined set of precoders, a.k.a. codebook-based precoding

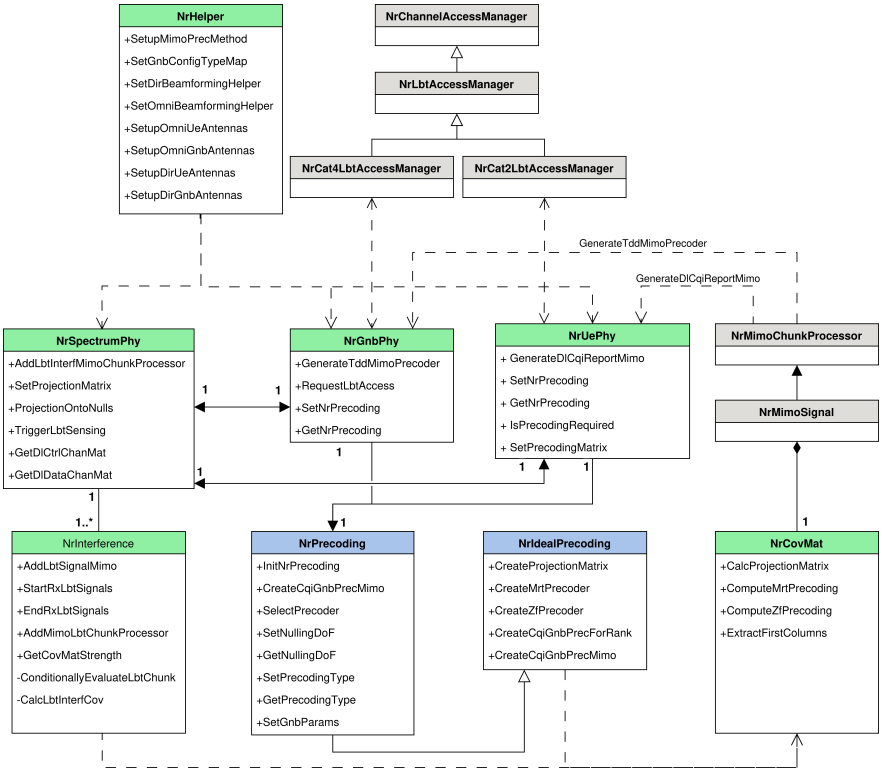

Figure 2: Diagram of Framework Used for DL Precoder for Beamforming with Radiation-Null Steering

projection onto the null channel subspaces of interference is enabled, `NrGnbPhy` sets the projection matrix within its associated `NrSpectrumPhy` class instance by calling `SetProjectionMatrix`.

`NrSpectrumPhy` serves as the link between NR PHY entities (gNB or UE) and the ns-3 spectrum channel, managing control and data transmissions, signal decoding, and interference identification. It interfaces with `NrInterference` for interference calculations and coordinates HARQ procedures. Each PHY entity maintains a `NrSpectrumPhy` instance, registering it with the spectrum channel to enable signal reception.

For this work, `NrSpectrumPhy` was extended to support an additional `NrInterference` instance dedicated to interference received during LBT. In `StartRx`, if a sensing gNB needs a null-projection matrix, incoming signals during LBT are processed as interference. If the projection matrix is available during this step, `ProjectionOntoNulls` applies projection to the incoming signal, recalculates the signals' power, and forwards them to the associated `NrInterference`. Lastly, a new method, `GetDlDataChanMat`, provides the gNB–UE forward (DL) channel matrix required for accurate precoding.

To efficiently handle multi-dimensional MIMO signals, the associated `NrInterference` class extends the basic Gaussian interference model inherited from LTE by accumulating incoming interference power. This class integrates the newly developed function `NrMimoChunkProcessor`, designed specifically for MIMO signal handling [3]. Unlike conventional SISO interference models, `NrMimoChunkProcessor` preserves detailed signal information without premature averaging, allowing precise downstream calculations.

To enable interference-plus-noise covariance matrix computations, essential for computing the projection matrix, new functionalities were added to the `NrInterference` class, such as the `AddMimoLbtChunkProcessor` method. This method manages instances of `NrMimoChunkProcessor`, each responsible for handling incoming interference signals during the LBT sensing phase. The methods `StartRxLbtSignals` and `EndRxLbtSignals` initiate and conclude interference signal processing. Upon successful LBT completion, the associated methods `ConditionallyEvaluateLbtChunk` and `CalcLbtInterfCov` compute the interference-plus-noise covariance matrix based on the collected interference signals. Completion of processing (`NrMimoChunkProcessor::End`) triggers a callback to the function `NrGnbPhy::GenerateTddMimoPrecoder`, providing the interference covariance matrix for further processing.

3.3 Precoding Framework and Class Extensions

This work introduces two new classes, `NrPrecoding` and its subclass `NrIdealPrecoding`, to ns-3, enabling advanced precoding functionalities based on perfect channel knowledge. `NrPrecoding` serves as a flexible interface for various precoding techniques (e.g., Maximum Ratio Transmission (MRT), Zero-Forcing (ZF), and their projection-based variants ProjectedMrt and ProjectedZf). It allows

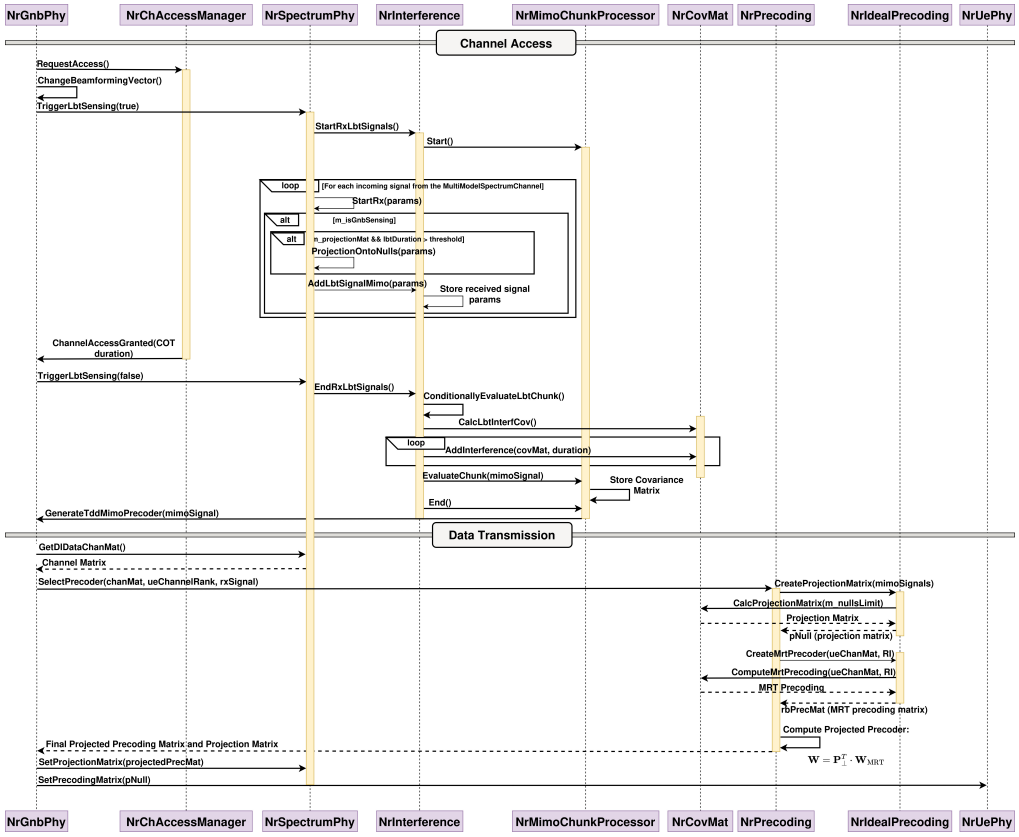

Figure 3: Sequence Diagram of the DL Precoder for Beamforming with Radiation-Null Steering: Maximum Ratio Transmission with Radiation-Null Steering

configuring the precoding method and specifying how many DoF[5] (`NullsLimit`) are reserved for interference nulling. Through its main method, `SelectPrecoder`, `NrPrecoding` can dynamically select and compute the appropriate precoding matrix.

The subclass `NrIdealPrecoding`, inheriting from `NrPrecoding`, assumes perfect knowledge of the channel state information (CSI). It provides methods like `CreateMrtPrecoder` and `CreateZfPrecoder` to generate precoding matrices through Hermitian transposition or matrix inversion of the known channel, respectively. Additionally, it supports null-space projection with `CreateProjectionMatrix`, leveraging eigenvalue decomposition from an extended `NrCovMat` class.

To facilitate the various computations, `NrCovMat` was significantly extended. The method `CalcProjectionMatrix` uses eigenvalue decomposition on the interference-plus-noise covariance matrix, identifying dominant interference directions and creating the null-projection matrix. Meanwhile, `ComputeMrtPrecoding` and `ComputeZfPrecoding` provide efficient matrix-based implementations of MRT and ZF precoders, respectively, using the Eigen library.

[5]Here, DoF refers to the number of independent spatial dimensions available for transmission, beamforming, or interference suppression.

3.4 Procedure for Sensing-Assisted Precoding with Radiation-Null Steering

Figure 3 depicts the sequence of interactions between key classes when computing a projected MRT precoder (i.e., MRT with radiation-null steering). The sequence begins with the gNB initiating an LBT procedure for channel access and concludes with the application of a projected MRT precoder upon successful channel access. The projection matrix will shape the precoder so that radiation-nulls are placed towards/from interfering nodes of which channels are received during the LBT sensing.

When the gNB has data to transmit and the channel is not yet granted, it calls `RequestAccess` in the `NrChannelAccessManager`. If precoding is enabled, the gNB updates its beamforming vector (`ChangeBeamformingVector`) for directional sensing and invokes `TriggerLbtSensing(true)` to begin the LBT procedure.

During the first stage, `NrSpectrumPhy` performs standard directional sensing for at least 0.3 ms (see "threshold" in Figure 3), capturing incoming signals via `StartRxLbtSignals` in `NrInterference`, which activates the `NrMimoChunkProcessor` for signal storage and processing. The accumulated samples are then used to estimate the interference-plus-noise covariance matrix and compute the projection matrix for null placement.

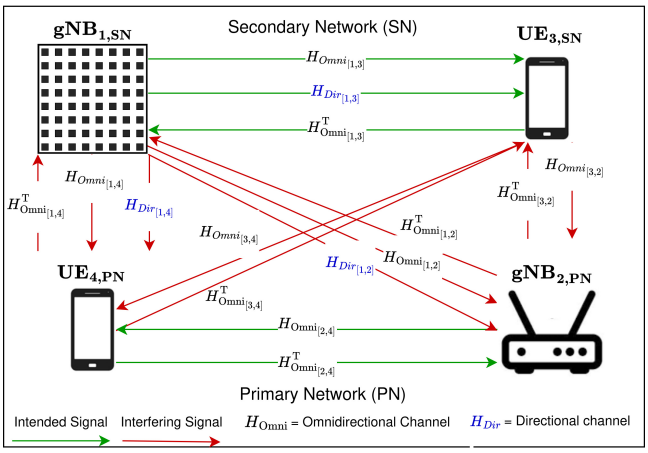

Figure 4: Wireless Channels: Intended (Green) and Interfering (Red) Links Between Primary and Secondary Network

In the second stage, the projection matrix is applied to incoming signals using `ProjectionOntoNulls(params)`, which actively suppresses energy from the dominant interference directions. The call to `AddLbtSignalMimo(params)` continues to store signal parameters for further analysis.

Once LBT deems the channel free according to Eq. 7, after validating that the projection matrix sufficiently suppresses all interference during the mandatory backoff period, in compliance with regulatory requirements, `NrChannelAccessManager` grants access and triggers `NrGnbPhy::ChannelAccessGranted`. Sensing is then stopped via `TriggerLbtSensing(false)`, and the final interference covariance is computed by `ConditionallyEvaluateLbtChunk()` and `CalcLbtInterfCov()`, with `AddInterference(signal)` finalising the process.

With the channel granted and the covariance matrix available, `NrGnbPhy::GenerateTddMimoPrecoder` is invoked. The gNB obtains the DL channel matrix for a given UE via `GetDlDataChanMat()` and calls the function `SelectPrecoder(chanMat, ueChanRank, rxMimoSignals)` to compute the final projected MRT precoder. First, the function `CreateProjectionMatrix(interfCovMat)` will call the function `CalcProjectionMatrix` to derive a projection matrix of the null channel subspaces of the strongest interference eigenmodes (i.e., interference directions) as shown in Eq. 2 and Eq. 3. Next, `CreateMrtPrecoder(chanMat)` constructs the baseline MRT beamformer (see Eq. 4), and the two matrices are processed to produce the final null-projected MRT precoder (see Eq. 5). The projected precoder and the projection matrix alone are then distributed to the gNB, which then sets the UE PHY layers by `SetPrecodingMatrix()` and the gNB associated NrSpectrumPhy instance with `SetProjectionMatrix()`, respectively.

By dynamically updating its beamformer based on sensed interference directions every time it initiates the channel (e.g., every 8, 4 or 2 ms), this sensing-assisted procedure mitigates interference via null projection. As shown in the diagram, `NrGnbPhy`, `NrSpectrumPhy`, `NrInterference`, `NrMimoChunkProcessor`, and the precoding-related classes work in unison to ensure that the final beamformer maximally strengthens the desired signal while nulling out dominant interference paths.

Table 1: Intended and Interfering Signal Power with Selected Channels in R_{intf} Measured During (a) Quasi-Omnidirectional and (b) Directional Sensing

(a)

Channels	P_{intf} [dBm]		P_{intf} [dBm]		$P_{intended}$ [dBm]
in R_{intf}	$gNB_{2,PN}$	$UE_{4,PN}$	$gNB_{2,PN} \rightarrow gNB_{1,SN}$	$UE_{4,PN} \rightarrow gNB_{1,SN}$	$UE_{3,SN}$
$H_{Omni[1,2]}$	-71.3	-81.8	-377.7	-82.6	-27.1
$H_{Omni[1,4]}$	-73.9	-92.9	-70.1	-368.4	-29.7
$H_{Omni[1,2]}$, $H_{Omni[1,4]}$	-72.9	-92.9	-373.9	-363.4	-32.1
MRT baseline	-82.8	-79.0	-66.3	-80.8	-24.7

(b)

Channels	P_{intf} [dBm]		P_{intf} [dBm]		$P_{intended}$ [dBm]
in R_{intf}	$gNB_{2,PN}$	$UE_{4,PN}$	$gNB_{2,PN} \rightarrow gNB_{1,SN}$	$UE_{4,PN} \rightarrow gNB_{1,SN}$	$UE_{3,SN}$
$H_{Omni[1,2]}$	-379.7	-78.9	-372.1	-80.1	-24.7
$H_{Omni[1,4]}$	-81.3	-392.2	-66.1	-368.4	-32.0
$H_{Omni[1,2]}$, $H_{Omni[1,4]}$	-378.3	-366.3	-372.5	-369.2	-34.3
MRT baseline	-82.8	-79.0	-66.3	-80.8	-24.7

4 Validation and Evaluation of Directional Sensing and Beamforming with Null Steering

To validate and evaluate the proposed null projected BF and channel access, we use the open-source ns-3 network simulator (ns-3.42) and the open-source 5G-LENA NR module (v3.1). For both the validation and evaluation, we consider a simple scenario with two networks, PN and SN, each with a single gNB and a single UE. The UE from the PN or SN are served with 1 data stream only. The PN gNB, UE and SN UE operate on omnidirectional transmission and are equipped with isotropic antenna elements. The SN is based on a high-performance gNB equipped with a single-panel, 16-port phased antenna array, configured as a 4×4 ($M = 4, N = 4$) UPA capable of digital precoding and directional data transmission. The SN gNB applies the DL precoding method detailed in Section 2 to prevent energy radiating towards/from the PN gNB and UE. The radio frame structure follows the transmission at a numerology of 30 kHz, with an S-Type slot structure [7] for a DL-only transmission of constant bit rate traffic of 82 Mbps.

4.1 Validation of Interference Nulling

To validate and explain the precoding procedure with radiation-null steering at the SN gNB, we use measurements of the power for the intended and interfering signals. These measurements demonstrate how omnidirectional versus directional sensing influences the effectiveness of the radiation-null steering. The scenario under consideration is depicted in Figure 4, where two NR-U gNBs share the same unlicensed band, each serving a single UE. One network (the PN) employs omnidirectional sensing and transmission, while the other (the SN) uses directional sensing and transmission. Figure 4 illustrates both the intended (green) and interfering (red) channels for every possible link, while the same channel notation is also used in Table 1 (a) and (b).

In a standard 5G-LENA NR setup, control signals are transmitted omnidirectionally by default. Consequently, even nodes that use directional transmissions for data still affect the wireless environment omnidirectionally during transmission of control signalling.

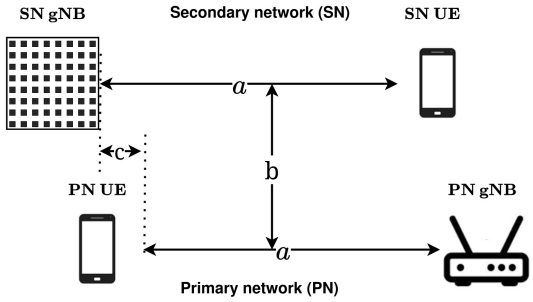

Figure 5: Spectrum Sharing Scenario: Primary Network (QuasiOmni) and Secondary Network (Directional)

The intended links are: (i) PN's DL $\mathbf{H}\text{Omni}[2,4]$ (and its UL transpose), and (ii) SN's DL, which combines a directional data channel $\mathbf{H}\text{Dir}[1,3]$ with an omnidirectional control channel $\mathbf{H}\text{Omni}[1,3]$ (also used in UL). Interference is observed: (a) at the SN gNB from PN UE and PN gNB via $\mathbf{H}\text{Omni}[1,4]^T$ and $\mathbf{H}\text{Omni}[1,2]^T$; (b) at the SN UE from PN gNB and UE via $\mathbf{H}\text{Omni}[3,2]$ and $\mathbf{H}\text{Omni}[3,4]$; (c) at the PN gNB from SN gNB's omnidirectional control $\mathbf{H}\text{Omni}[2,1]^T$; and (d) at the PN UE from the SN gNB's directional and omnidirectional paths $\mathbf{H}\text{Dir}[1,4]$ and $\mathbf{H}\text{Omni}[1,4]$

To evaluate how beam-nulling performance depends on sensing directionality, we measure both the desired power at the SN UE and the interfering power at the SN gNB, PN gNB, and PN UE for each data transmission. To show specific null placement (e.g., during the LBT sensing only signals from specific nodes are captured), we introduced targeted (hard-coded) modifications. Table 1(a) and (b) list the measured power when the interference-plus-noise covariance matrix $\mathbf{R_{intf}}$ is computed under directional and omnidirectional sensing, respectively, while $\mathbf{R_{intf}}$ contains only certain channel(s).

In Table 1 (a), the SN gNB performs omnidirectional sensing during LBT, meaning the interfering signals used to form $\mathbf{R_{intf}}$ arrive via $\mathbf{H}_{\text{Omni}[1,2]}$ and $\mathbf{H}_{\text{Omni}[1,4]}$. Under these conditions, when a PN signal is detected, the measured interference at the SN gNB becomes negligible. However, in comparison to the MRT baseline, the SN UE shows a reduced received power, indicating a decrease in beamforming gain from its serving gNB. This degradation increases if $\mathbf{R_{intf}}$ includes channels from both PN nodes, as more DoF will be allocated to cover all interference directions, leaving fewer resources for the intended BF gain.

Turning to the PN nodes, Table 1(a) shows that the interfering power at the PN gNB or PN UE has a slight decrease or increase. For instance, consider the PN UE ($\text{UE}_{4,\text{PN}}$) when omnidirectional LBT sensing captures signals on $\mathbf{H}_{\text{Omni}[1,4]}$ from the PN UE to SN gNB ($\text{gNB}_{1,\text{SN}}$). Although the SN gNB effectively nulls the UL interference, significantly reducing the power at $\text{gNB}_{1,\text{SN}}$, the power at the PN UE remains largely unchanged relative to the MRT baseline. In essence, if $\mathbf{R_{intf}}$ is computed based on signals received on the omnidirectional channels, SN gNB only suppresses interference arriving *from* the PN UE; it does not address the interference *toward* it. Because the SN gNB senses interference only via $\mathbf{H}_{\text{Omni}[1,4]}$, the PN UE continues to be affected by the energy from the directional data transmission on $\mathbf{H}_{\text{Dir}[1,4]}$, due to distinct phase and magnitude characteristics that are not captured in omnidirectional sensing. Consequently, only the SN gNB benefits from nulling in this case.

Table 2: Scenario Configuration Parameters

Parameter name	Parameter value
ns-3 simulator release	Release 41
5G-LENA NR module	Release v3.1 [5]
Independent random simulation runs	100 repetitions per setup (ns-3 RNG values: 1–100)
Simulation time	1 s
Type of traffic	DL Constant Bit Rate (CBR)
CBR inter-packet interval time	100 μs
CBR packet size	1000 bytes
Channel model	3GPP TR 38.901 InH
Channel update period	0 ms
LoS/NLoS condition model	3GPP TR 38.901 InH
LoS/NLoS update period	0 ms
Central frequency	5.22 GHz
Bandwidth	20 MHz
SN/PN gNB and UE transmit power	24 dBm and 18 dBm
SN gNB	Uniform Planar Array 3GPP
SN UE, PN gNB and UE	Isotropic Antenna Model
MIMO Precoding	MRT or MRT with radiation-null steering (Eq. 5)
SN gNB	Single-Panel
SN gNB	$M = 4$, $N = 4$, $d_h = 0.5\lambda$, $d_v = 0.5\lambda$, $N_h = 4$, $N_v = 4$
PN or SN gNB	1 spatial layer
PN or SN gNB and UE antenna height	3 and 1 m
PN or SN gNB and UE noise figure	5 dB and 9 dB
SN gNB and PN UE or SN gNB and UE antenna gain	8 dBi (max) and 0 dBi
Numerology	1 (30 kHz subcarrier spacing)
Duplexing mode	TDD
Multiple access scheme	TDMA
TDD subframe pattern	Special (S|S|S|S|S|S|S|S|S|S)
TDD slot format	DL|DL|DL|DL|DL|DL|DL|DL|DL|UL
MCS Table	Table 2, TS 38.214 Table 5.1.3.1-2
HARQ combining method	Incremental redundancy
Max no. of HARQ processes	20
Max no. of HARQ retx	3
UE processing delay (K1)	2 slots
RLC mode	Unacknowledged mode
Shared Channel Access	Type 1 CAP with priority p4, ED of -72dBm

In Table 1(b), by contrast, the SN gNB relies on directional sensing for LBT and $\mathbf{R_{intf}}$ computation. Now, the interfering signals from the PN are received over $\mathbf{H}_{\text{Dir}[1,2]}$ and $\mathbf{H}_{\text{Dir}[1,4]}$, which are the same channels through which the PN nodes receive data interference from the SN gNB. As a result, the power at the PN gNB or PN UE becomes negligible when the relevant channel is included in $\mathbf{R_{intf}}$, demonstrating that the projection matrix computed during directional sensing can simultaneously mitigate the interference *towards* and *from* the PN network.

4.2 Evaluation of Interference Nulling

For the evaluation of the proposed technique, certain characteristics in the simple scenario will be varied to evaluate the efficiency of the null projected BF when using a fixed number of DoF for null steering. Key performance metrics such as throughput and latency will be used to analyse the coexistence of a PN and SN for various transmission configurations, including QuasiOmni coexisting with QuasiOmni; QuasiOmni coexisting with CellScan using an MRT precoder; and QuasiOmni coexisting with CellScan using an MRT precoder combined with radiation-null steering with different degrees of freedom (DoF) assigned for nulling.

This section evaluates the throughput and latency performance of the PN and SN under varying interference levels using the simple deployment scenario depicted in Figure 5. To reproduce a varying level of interference, we vary the distance b shown in Figure 5 from 5 m to 120 m while distance a is kept constant at 10m. Due to the geometry of the phased antenna array used by the SN gNB, an offset c of 3m is introduced. This offset is necessary since a single-panel

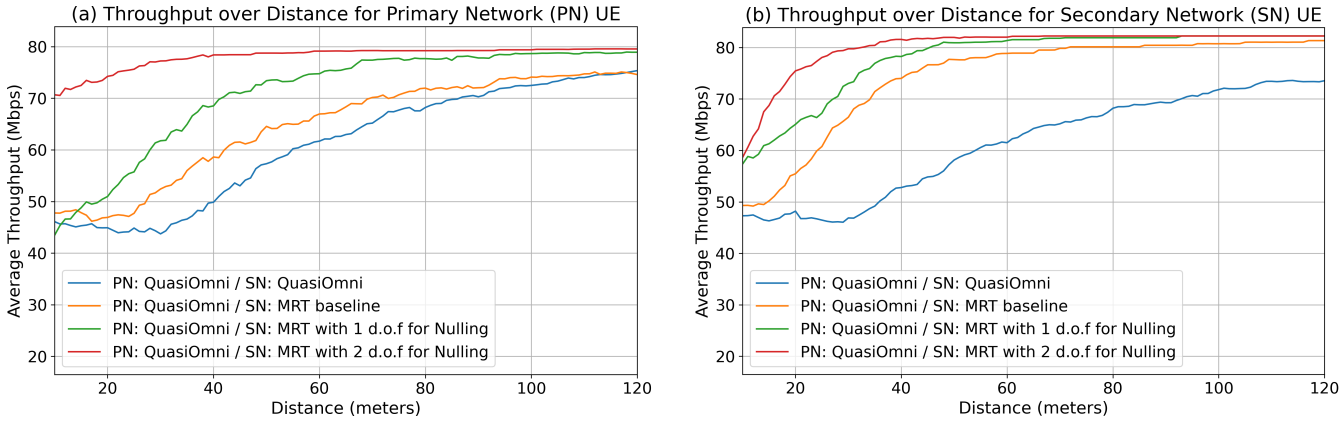

Figure 6: Average Throughput Versus Distance: (a) Primary Network; (b) Secondary Network

UPA cannot efficiently detect signals arriving parallel to the array panel.

4.2.1 Throughput Analysis for Primary and Secondary Networks. This subsection evaluates the throughput performance of both the PN and SN under varying distance b (see Figure 5) between the interfering links and also under different transmission methods implemented by the SN gNB. Figures 6a and 6b illustrate the average throughput for PN and SN UEs, respectively, across different SN gNB transmission modes: QuasiOmni (baseline), MRT baseline (see Eq. 4), MRT with 1 and 2 DoF for nulling (see Eq. 5). The results highlight the interplay between spatial reuse efficiency, interference suppression, and signal degradation.

Figure 6a shows the PN throughput as a function of distance (5 to 120 m) when coexisting with the SN where the gNB implements various transmission modes. When the SN gNB operates in QuasiOmni mode, the PN throughput decreases sharply, while after $b = 30\ m$, an ascending trend is observed. When the MRT baseline is used at the SN gNB, an overall throughput enhancement is observed, which is attributed to the directionality of the transmission. Furthermore, Figure 6a shows that throughput degradation at close proximity is reduced when the SN gNB uses the MRT baseline compared to the QuasiOmni. While an increase in achieved throughput is observed across all distances, the improvement becomes more substantial beyond $b = 14$ m. Finally, the data reveals that for neither QuasiOmni nor MRT baseline is the maximum 82 Mbps data rate achieved, even at the largest tested distance of $b = 120$ m.

When the SN gNB employs null-projected MRT with 1 DoF, allocating one antenna port to suppress a dominant interference direction, the PN achieves a net throughput gain compared to QuasiOmni and MRT baseline configurations. However, this improvement comes with a slight throughput degradation for the PN when operating in close proximity to the SN. This degradation is explained by the insufficient DoF available to null interfering directions. Given that a DL-only scenario is used, signals captured during LBT sensing and used to compute the projection matrix (see Eq. 3) are primarily control and data signals from the PN gNB, while the PN UE occasionally sends uplink control information (UCI). This leads to null steering towards/from the PN gNB and not its UE, which allows the completion of the LBT procedure at the PN gNB. However, since the SN gNB only creates nulls towards the PN gNB, the PN UE remains under high interference, resulting in poor link reliability. Given this limitation, projection-based precoding with 1 DoF still leads to higher PN throughput performance after a distancing of $b > 14\ m$.

Notably, when the SN gNB uses 2 DoF, the projected precoding provides the best performance at any distance b. This shows that when enough DoF are provided, the SN gNB can prevent any interference towards/from the PN for any data transmission, allowing a perfect throughput to be achieved. The slight degradation at close proximity is due to the omnidirectionally transmitted control signals and the signals transmitted by the SN UE.

Figure 6b reveals distinct throughput trends for the SN under different precoding configurations. The QuasiOmni mode achieves the lowest throughput due to unmitigated interference, while the MRT baseline improves performance by focusing energy toward the SN UE. The projected MRT precoding, with 1 or 2 DoF allocated for interference nulling, exhibits a critical trade-off: despite suppressing all dominant interference directions (2 DoF for the 2 PN nodes), significant throughput degradation occurs at close proximity ($b < 9\ m$) to the PN. Allocating DoF to spatial nulls reduces BF gain toward the SN UE but chiefly benefits the primary network: interference at PN nodes is suppressed, and the SN gNB senses low energy from the nulled directions (i.e., PN nodes), typically below the LBT threshold, allowing its backoff to clear more frequently. The SN UE benefits indirectly via its gNB's improved channel access probability but may suffer SNR loss when many degrees of freedom (DoF) are used for nulling, especially without receiver post-processing, as seen for the 2 DoF case at small b distance in Figure 6b. At distances $b < 9\ m$, this configuration reduces SN UE throughput due to the precoder prioritising nulling over beamforming gain, weakening the desired link, and the SN UE's exposure to high interference from the PN without UE-side post-processing.

4.2.2 Latency Analysis for Primary and Secondary Networks. This subsection examines the average and median latency for both the PN and SN when the SN gNB employs various precoding schemes

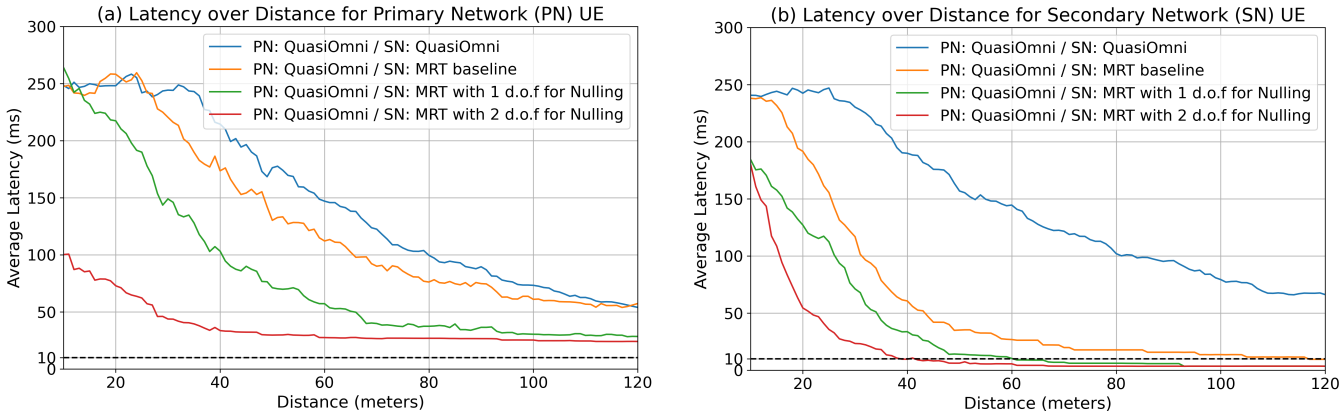

Figure 7: Average Latency Versus Distance: (a) Primary Network; (b) Secondary Network

or QuasiOmni transmission. Our focus is on how each approach impacts latency at different levels of interference, achieved by varying the distance b in the deployment illustrated in Figure 5.

Figure 7a illustrates the PN latency versus distance for different SN transmission strategies. When comparing QuasiOmni and the MRT baseline, both yield similar PN latency at shorter distances. As distance b increases, however, MRT's directional properties help reduce PN mean latency more effectively: QuasiOmni begins to improve at about $b > 32$ m, while the MRT baseline requires distances beyond $b > 22$ m for noticeable gains.

When the SN gNB uses projected MRT with 1 degree of freedom (DoF) for nulling, the PN undergoes the highest latency at very short distances ($b < 10$ m) because the projection-based precoder mainly captures the PN gNB signal, thereby exposing the PN UE to stronger interference. By contrast, adding sufficient DoF (i.e., 2 DoF) alleviates interference and lowers PN latency. Even then, meeting the 10 ms latency, which is a common latency requirement, remains difficult when considering worst-case average latency. Focusing on the median (50th percentile) latency, QuasiOmni maintains latency under 10 ms at $b > 70$ m, MRT baseline achieves it at $b > 48$ m, MRT with 1 DoF does so at $b > 38$ m, and MRT with 2 DoF meets it at $b > 28$ m.

Figure 7b shows the SN latency under the same set of SN precoding techniques. As with the PN, QuasiOmni produces the highest latency, followed by the MRT baseline and projected MRT with 1 and 2 DoF. The 10 ms latency requirement, the average SN latency falls below 10 ms at $b > 16$ m for the MRT baseline, $b > 60$ m for MRT with 1 DoF, and $b > 38$ m for MRT with 2 DoF. Median results indicate that QuasiOmni requires $d > 79$ m to dip below 10 ms, MRT baseline meets this threshold at $d > 31$ m, MRT with 1 DoF does so at $d > 29$ m, and MRT with 2 DoF at $d > 15$ m.

5 Conclusion

Our results confirm that employing MRT with radiation null steering in an NR-U coexistence scenario significantly improves throughput and reduces latency for both the primary and secondary networks. Allocating a number of DoF equal to the number of active interfering devices for null placement enhances spectral efficiency by allowing both networks to access the same channel concurrently and perform simultaneous successful transmissions.

Acknowledgments

CTTC authors have received funding from Grant PID2021-126431OB-I00 funded by MCIN/AEI/10.13039/501100011033 and "ERDF A way of making Europe", and Generalitat Catalunya 2021 SGR 00770.

References

[1] 3GPP TSG RAN. 2018. Study on NR-based Access to Unlicensed Spectrum. 3GPP TR 38.889 V16.0.0. https://www.3gpp.org/ftp/Specs/archive/38_series/38.889/
[2] 3GPP TSG RAN. 2024. Physical Layer Procedures for Shared Spectrum Channel Access. 3GPP TS 37.213 V18.3.0. https://www.3gpp.org/ftp/Specs/archive/37_series/37.213/
[3] Biljana Bojović and Sandra Lagén. 2025. 3GPP-Compliant Single-User MIMO Model for High-Fidelity Mobile Network Simulations. *Computer Networks* 256 (2025), 110912.
[4] Ericsson AB. 2024. 6G Spectrum: Enabling the Future Mobile Life Beyond 2030. White Paper. Available: https://www.ericsson.com/en/reports-and-papers/white-papers/6g-spectrum-enabling-the-future-mobile-life-beyond-2030.
[5] Guilherme Ferreira, Biljana Bojović, Konstantina Koutlia, Ali Ashtari, Andoni Larrañaga, Sandra Lagén, Nicola Patriciello, Ziaul Ali, and Luca Giupponi. 2024. 5G-LENA ns-3 NR Module, Release 3.1, 5g-lena-v3.1.y.
[6] George V. Frangulea, Philippos Assimakopoulos, Biljana Bojović, and Sandra Lagén. 2024. NR-U and Wi-Fi Coexistence in Sub-7 GHz Bands: Implementation and Evaluation of NR-U Type 1 Channel Access in ns-3. In *Proceedings of the 2024 Workshop on ns-3*. ACM, Castelldefels, Spain, 36–44.
[7] George V. Frangulea, Philippos Assimakopoulos, Biljana Bojović, and Sandra Lagén. 2025. NR-U and Wi-Fi Unlicensed Spectrum Sharing: Design Challenges and Solutions. *Computer Communications* 237 (2025), 108143. doi:10.1016/j.comcom.2025.108143
[8] Giovanni Geraci, Alejandro Garcia Rodriguez, David López-Pérez, Andrea Bonfante, Leonardo Guido Giordano, and Holger Claussen. 2017. Operating Massive MIMO in Unlicensed Bands for Enhanced Coexistence and Spatial Reuse. *IEEE Journal on Selected Areas in Communications* 35, 6 (2017), 1282–1293.
[9] Konstantina Koutlia, Biljana Bojović, Ziaul Ali, and Sandra Lagén. 2022. Calibration of the 5G-LENA System Level Simulator in 3GPP Reference Scenarios. *Simulation Modelling Practice and Theory* 119 (2022), 102580.
[10] Nicola Patriciello, Sandra Lagén, Biljana Bojović, and Luca Giupponi. 2019. An E2E Simulator for 5G NR Networks. *Simulation Modelling Practice and Theory* 96 (2019), 101933.
[11] Radio Spectrum Policy Group. 2023. *The Development of 6G and Possible Implications for Spectrum Needs and Guidance on the Rollout of Future Wireless Broadband Networks.* Technical Report. European Radio Spectrum Policy Group. https://radio-spectrum-policy-group.ec.europa.eu/index_en.
[12] Radio Spectrum Policy Group (RSPG). 2025. *6G Strategic Vision: RSPG Report RSPG25-006 FINAL.* Technical Report. European Commission, DG CONNECT. Available: https://radio-spectrum-policy-group.ec.europa.eu/index_en.